Supplementary Information

Skin-friendly soft strain sensor with direct skin adhesion enabled by non-toxic surfactant

Haechan Park,‡[a] Myeonghyeon Na,‡[a] Donghyung Shin,‡[a] Daeun Kim,[a] Euna Kim,[b] Sehyun Kim,[a] Donghyun Lee,[b] Kyoseung Sim*[a,c]

[a]Department of Chemistry, Ulsan National Institute of Science and Technology (UNIST), Ulsan, 44919, Republic of Korea.

[b]School of Energy and Chemical Engineering, Ulsan National Institute of Science and Technology (UNIST), Ulsan, 44919, Republic of Korea.

[c]Center for Wave Energy Materials, Ulsan National Institute of Science and Technology (UNIST), Ulsan, 44919, Republic of Korea.

‡These authors contributed equally to this work.

*Correspondence to: kyos@unist.ac.kr

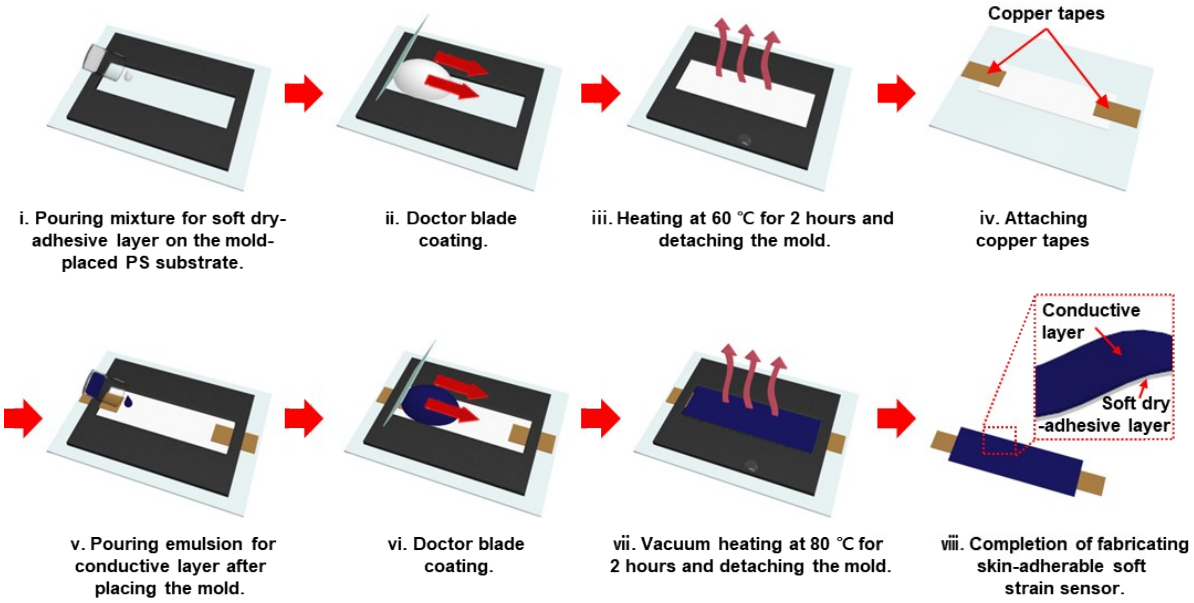

Fig. S1 A schematic fabrication process of the skin-adherable soft strain sensor.

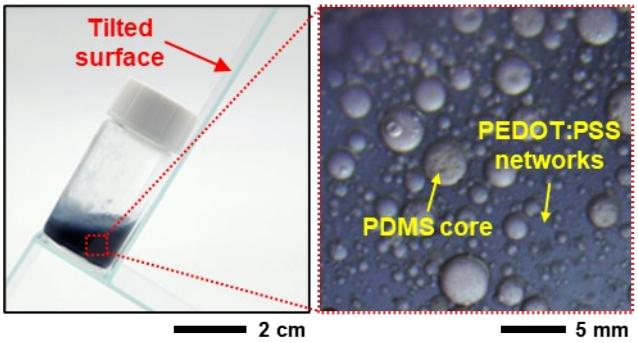

Fig. S2 Optical (left) and optical microscopic (right) images of the emulsions state of soft conductive composite blended with pristine PEDOT:PSS solution.

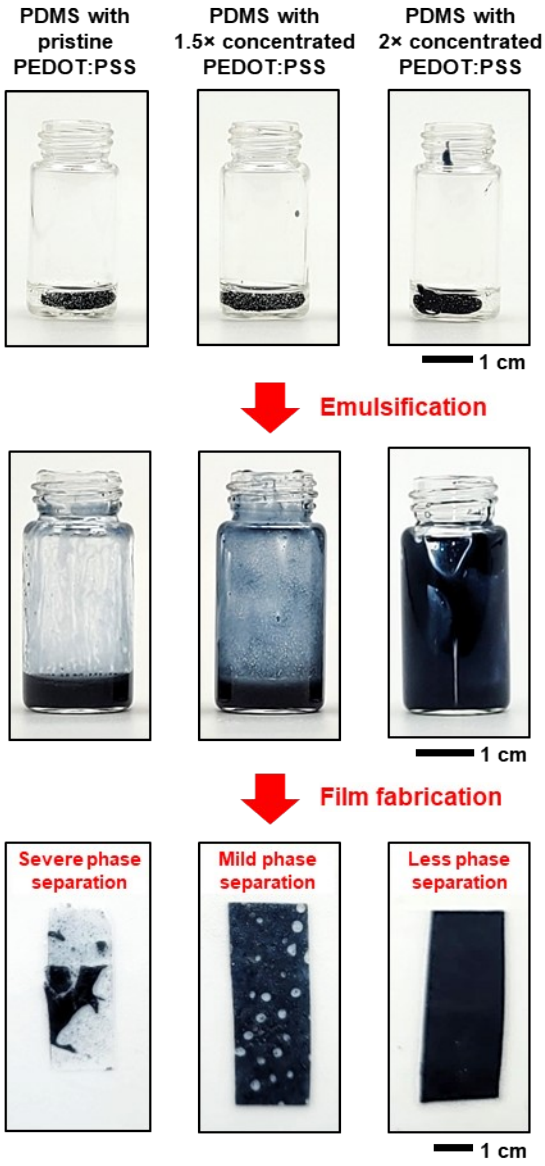

Fig. S3 Optimization process of concentrating PEDOT:PSS solution for the soft conductive composite.

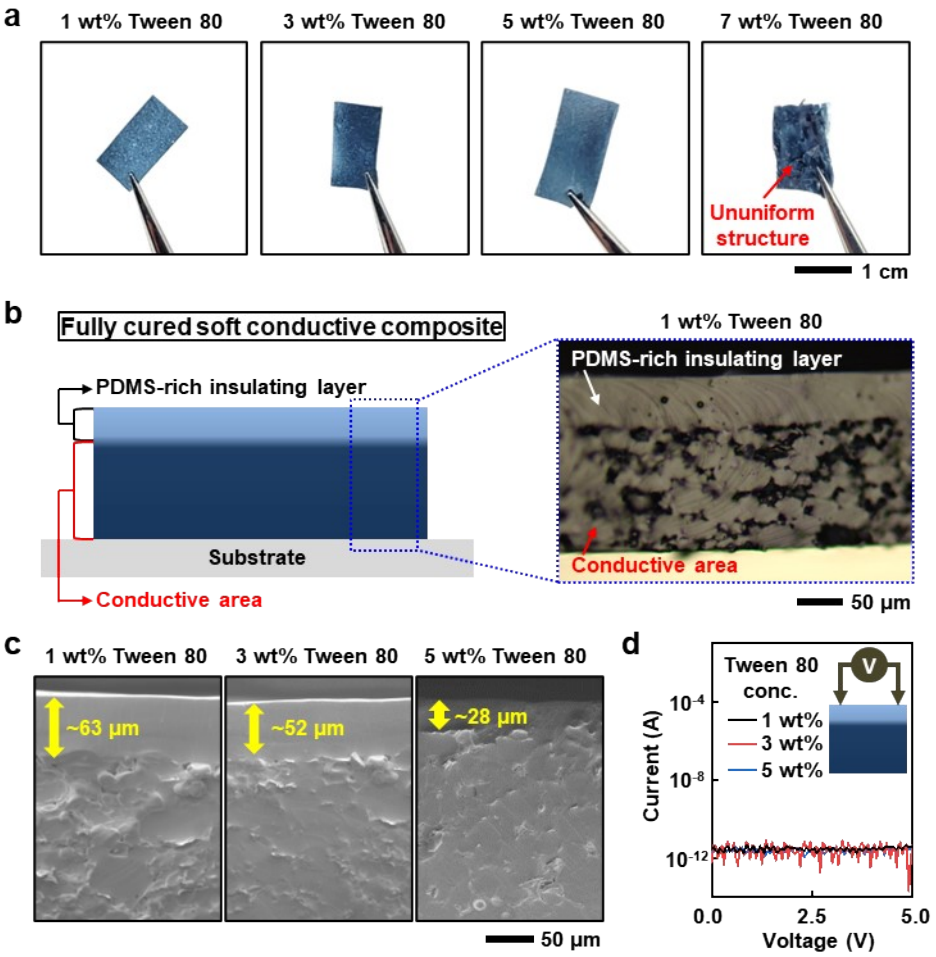

Fig. S4 Optimization process of Tween 80 concentration for the soft conductive composites. (a) Optical images of the soft conductive composite with varying Tween 80 concentrations. (b) Schematic illustration of the phase-separated soft conductive composites (left) and cross-sectional optical microscopic image (right) of the 1 wt% Tween 80-added soft conductive composites. (c) Cross-sectional SEM images of the soft conductive composites as a function of Tween 80 concentrations. (d) Current-voltage curves of the PDMS-rich insulating layers in the soft conductive composites, depending on the Tween 80 concentrations, with an inset showing a schematic illustration of the measurement setup.

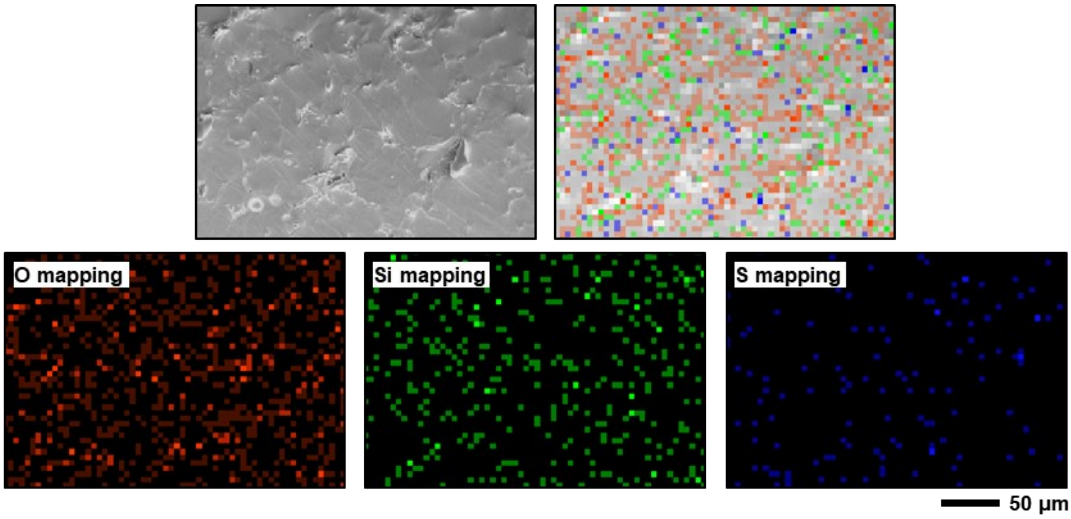

Fig. S5 Cross-sectional EDS elements mapping of the 5 wt% Tween 80-added soft conductive composite.

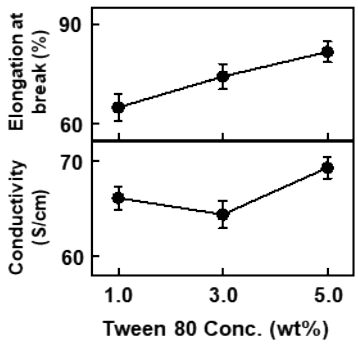

Fig. S6 Electrical conductivities (bottom) and elongation at break (top) of the soft conductive composites depending on the Tween 80 concentrations (n = 5).

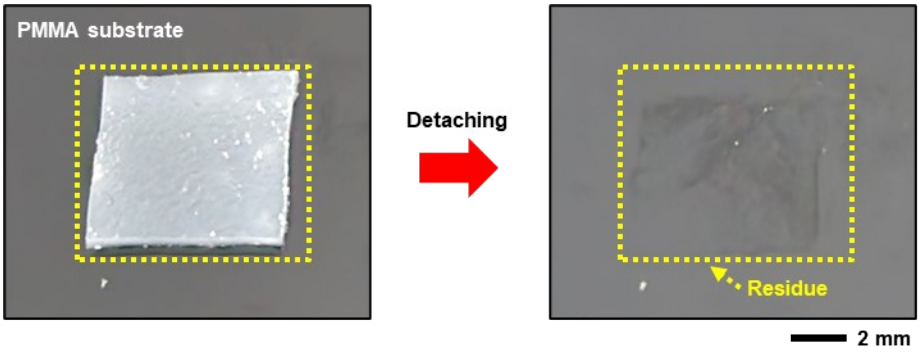

Fig. S7 Residue test of the 3.0 wt% Tween 80-added soft dry-adhesive film.

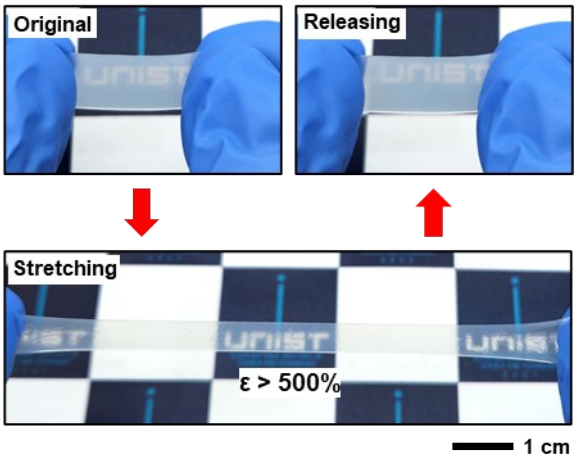

Fig. S8 Optical images of the 2.5 wt% Tween 80-added soft dry-adhesive film under mechanical strain.

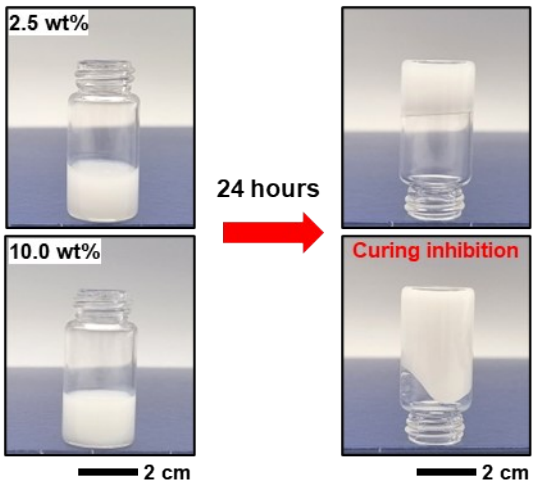

Fig. S9 Optical images of the 2.5 wt% (top), and 10.0 wt% (bottom) Tween 80-added soft dry-adhesive films curing at room temperature for 24 hours.

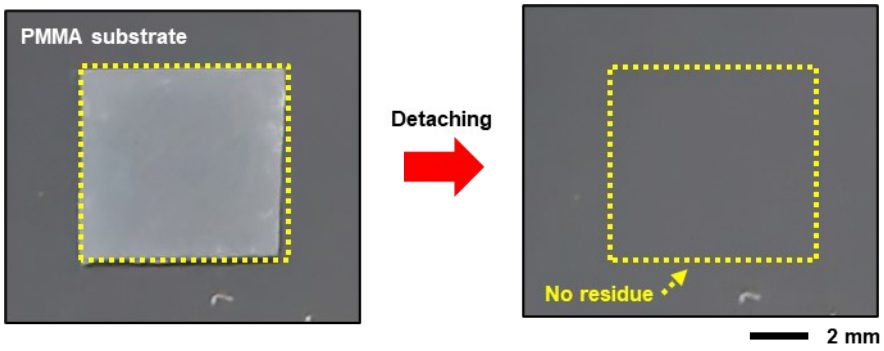

Fig. S10 Residue test of the 2.5 wt% Tween 80-added soft dry-adhesive film.

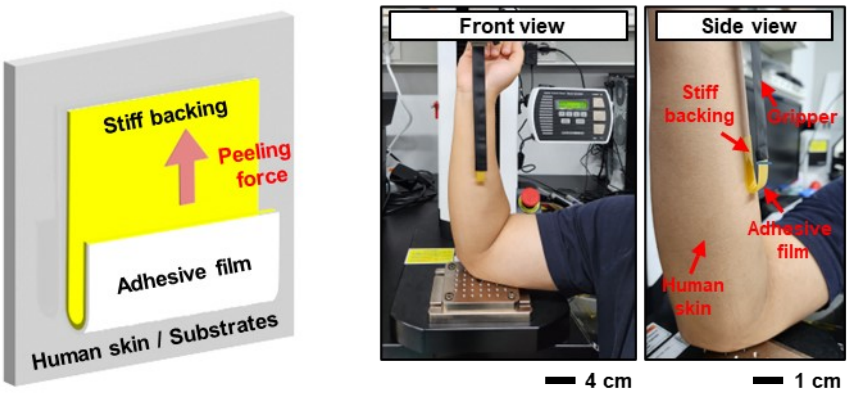

Fig. S11 Schematic (left) and optical (right) images of the adhesion test.

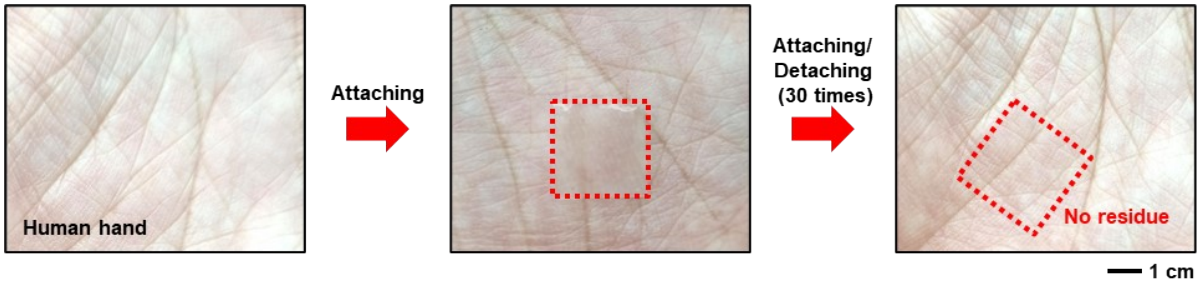

Fig. S12 Residue test of the 2.5 wt% Tween 80-added soft dry-adhesive film on human hand.

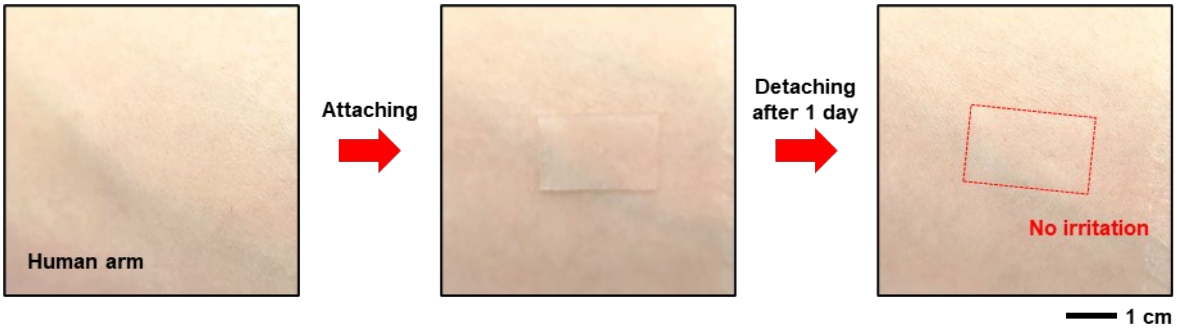

Fig. S13 Skin irritation test of the 2.5 wt% Tween 80-added soft dry-adhesive film on the human arm.

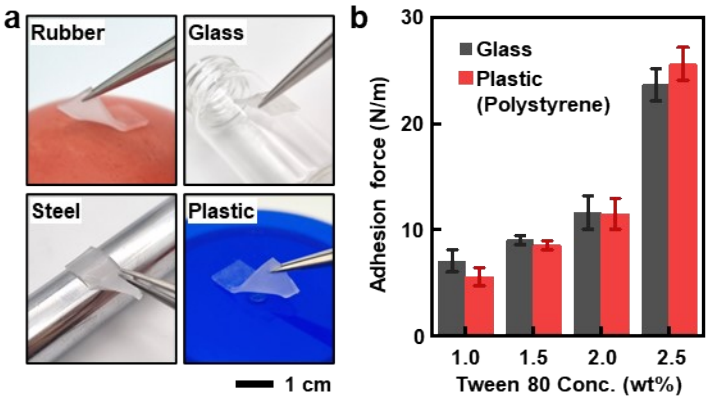

Fig. S14 Adhesion properties of the soft dry-adhesive film on the various objects. (a) Optical images of the 2.5 wt% Tween 80-added soft dry-adhesive film on the various subjects. (b) Adhesion forces of the soft dry-adhesive films with different Tween 80 concentrations on the various subjects (n = 5).

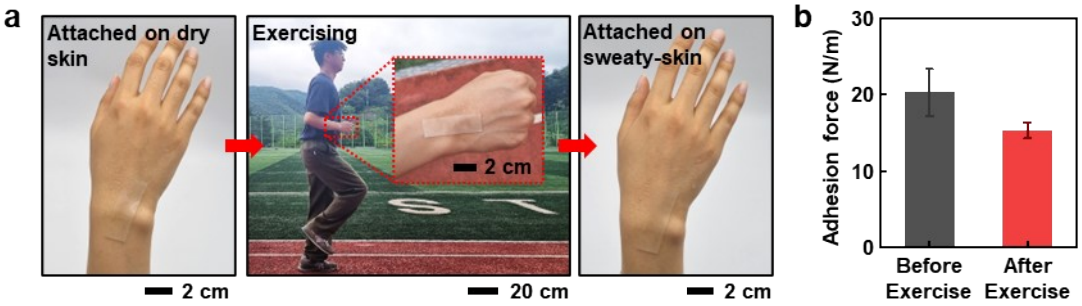

Fig. S15 Sweating effect on the adhesion force of the soft dry-adhesive film. (a) Optical images and (b) adhesion force of the soft dry-adhesive films before, and after exercising (n = 5).

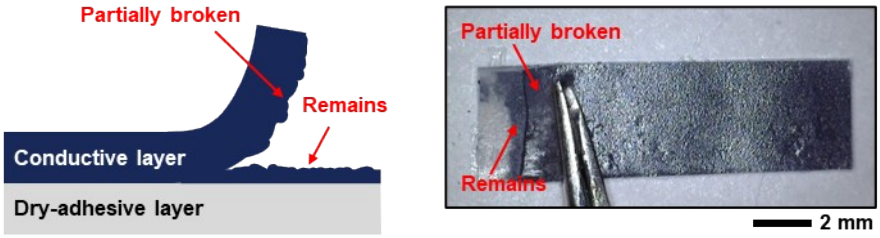

Fig. S16 Schematic (left), and optical (right) images of significant adhesion between conductive, and dry-adhesive layers.

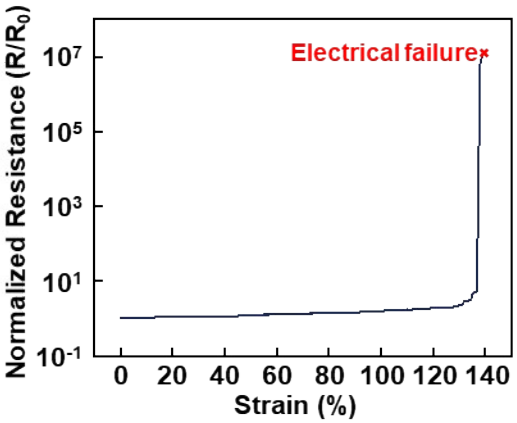

Fig. S17 Electrical failure of the skin-adherable soft strain sensor under the mechanical strain.